

Application of regional meteorology and air quality models based on MIPS and LoongArch CPU Platforms

Zehua Bai^{1,2}, Qizhong Wu^{1,2}, Kai Cao^{1,2}, Yiming Sun³, Huaqiong Cheng^{1,2}

¹College of Global Change and Earth System Science, Faculty of Geographical Science, Beijing Normal University, Beijing 100875, China.

²Joint Center for Earth System Modeling and High Performance Computing, Beijing Normal University, Beijing 100875, China.

³Beijing Institute of Talent Development Strategy, Beijing 100032, China.

Correspondence: Qizhong Wu (wqizhong@bnu.edu.cn)

Abstract. The Microprocessor without interlocked piped stages (MIPS) and LoongArch are Reduced Instruction Set Computing (RISC) processor architectures, which have advantages in terms of energy consumption and efficiency. There are few studies on the application of MIPS and LoongArch CPUs in the geoscientific numerical models. In this study, Loongson 3A4000 CPU platform with MIPS64 architecture and Loongson 3A6000 CPU platform with LoongArch architecture were used to establish the runtime environment for the air quality modelling system Weather Research and Forecasting–Comprehensive Air Quality Model with extensions (WRF-CAMx) in Beijing-Tianjin-Hebei region. The results show that the relative errors for the major species (NO₂, SO₂, O₃, CO, PNO₃ and PSO₄) between the MIPS and X86 benchmark platform are within $\pm 0.1\%$. The maximum Mean Absolute Error (MAE) of major species ranged to 10^{-2} ppbV or $\mu\text{g m}^{-3}$, the maximum Root Mean Square Error (RMSE) ranged to 10^{-1} ppbV or $\mu\text{g m}^{-3}$, and the Mean Absolute Percentage Error (MAPE) remained within 0.5%. The CAMx takes about 195 minutes on Loongson 3A4000 CPU, 71 minutes on Loongson 3A6000 CPU and 66 minutes on Intel Xeon E5-2697 v4 CPU, when simulating a 24h-case with four parallel processes using MPICH. As a result, the

30 single-core computing capability of Loongson 3A4000 CPU for the WRF-CAMx
31 modeling system is about one-third of Intel Xeon E5-2697 v4 CPU and Loongson
32 3A6000 CPU is slightly lower than Intel Xeon E5-2697 v4 CPU, but the thermal design
33 power (TDP) of Loongson 3A4000 is 40W, while the Loongson 3A6000 is 38W, only
34 about one-fourth of Intel Xeon E5-2697 v4, whose TDP is 145W. The results also verify
35 the feasibility of cross-platform porting and the scientific usability of the ported model.
36 This study provides a technical foundation for the porting and optimization of
37 numerical models based on MIPS, LoongArch or other RISC platforms.

38

39 **1 Introduction**

40 In the recent years, with the increasing demand for high-performance computing
41 resources and rapid development in the computer industry, especially supercomputer,
42 central processing unit (CPU) has undergone significant advancements in logical
43 structure, operational efficiency, and functional capabilities, making it the core
44 component of current computer technology development. There are two main types:
45 one is complex instruction set computer (CISC) CPU (George, 1990; Shi, 2008), mainly
46 using X86 architecture, representative vendors including Intel, AMD, etc., and widely
47 used in high-performance computing platforms. The other is reduced instruction set
48 computer (RISC) CPU (Mallach, 1991; Liu et al.,2022), mainly using ARM, MIPS,
49 RISC-V and other architectures, representative vendors including Loongson, etc., and
50 mainly used in high-performance computing platforms, which have high efficiency,
51 excellent stability and scalability. The Microprocessor without interlocked piped stages
52 (MIPS) architecture is one of the significant representatives of RISC architecture. MIPS
53 was originally developed in the early 1980s by Professor Hennessy at Stanford
54 University and his group (Hennessy et al., 1982). The simplicity of the MIPS instruction
55 set contributes to its ability to process instructions quickly, thus achieving higher
56 performance even in low-power conditions. In 1999, MIPS Technology Inc. released
57 the MIPS32 and MIPS64 architecture standard (MIPS Technology Inc., 2014).
58 Compared to the CISC CPUs, RISC CPUs demonstrate excellent performance and

59 power efficiency, which have gained popularity among chip manufacturers.

60 The Loongson processor family developed by Loongson Technology is mainly
61 designed using MIPS architecture and Linux operating system (Hu et al, 2011), which
62 has rich application tools in Linux open-source projects. The main reason that currently
63 restricts the development of CPUs that implement non-X86 instruction set architecture
64 such as MIPS64 is the immature software ecosystem (Hu et al., 2016). Based on the
65 strategy of open-source software, Loongson platform has gained abundant software
66 tools, making it possible to further develop scientific computing and numerical models.

67 Air quality model (AQM) systems use mathematical equations and algorithms to
68 simulate and predict the pollutant concentration in the atmosphere. The current AQMs
69 have become more complex, incorporating numerous factors such as emissions from
70 industrial sources, vehicle traffic, and natural sources, as well as meteorological
71 conditions, including modeling meteorology, emissions, chemical reactions, and
72 removal processes (Zhang et al., 2012). Regional-scale AQMs have been widely used
73 to predict air quality in cities, formulate emission reduction strategies, and evaluate the
74 effectiveness of control policies (Wang et al., 2023), including the Community
75 Multiscale Air Quality (CMAQ) modelling system (Appel et al., 2017; Appel et al.,
76 2021), the Comprehensive Air Quality Model with extensions (CAMx; RAMBOLL
77 ENVIRON Inc., 2014), and the Nested Air Quality Prediction Modeling System (Wang
78 et al., 2006; Chen et al., 2015). Due to the requirement of meteorological input,
79 commonly used offline meteorological models such as WRF (Michalakes et al., 2001)
80 are coupled offline with the regional AQMs to provide meteorological and chemical
81 forecast as the WRF-AQM modeling system, such the WRF-CMAQ modeling system
82 (Wu et al., 2014).

83 Both the meteorological and air quality numerical simulation rely heavily on high-
84 performance computing systems. The WRF-AQM systems can run stably on high-
85 performance computing platforms based on X86 or X86-compatible instruction set
86 architecture (ISA) CPUs, which account for the highest percentage among the main
87 processors of current high performance computing platforms. There are relatively
88 limited researches on the application of WRF-AQM system on MIPS and LoongArch

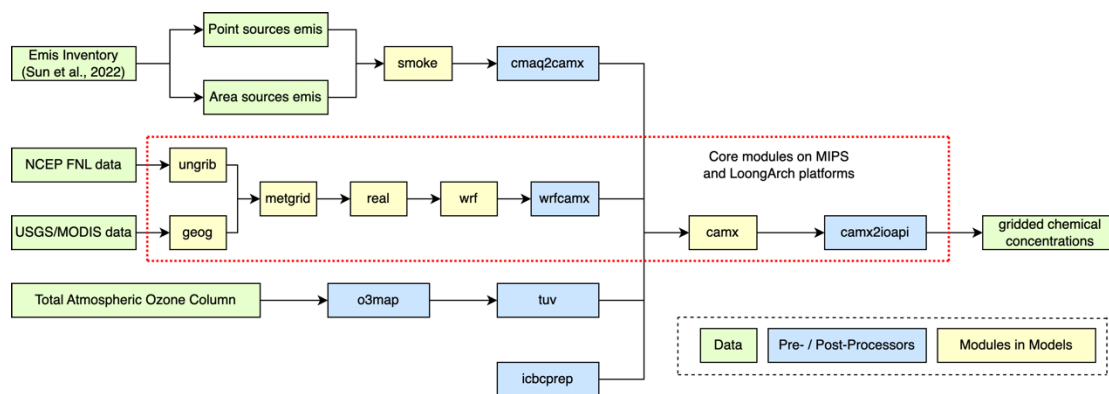
89 CPU platforms at present, this study focuses on the application of WRF-CAMx model
90 on Loongson CPU platform based on the MIPS and LoongArch architectures. A
91 simulation case covering the Beijing-Tianjin-Hebei region was set up to evaluate the
92 differences and performance between MIPS and X86 platforms. This study validated
93 the stability of scientific computing on MIPS and LoongArch CPU platform, and it
94 offered technical references and evaluation methods for the porting and application of
95 numerical models on non-X86 platforms.

96 Section 2 provides the model descriptions of the Weather Research and
97 Forecasting–Comprehensive Air Quality Model with extensions (WRF-CAMx)
98 modeling system, and the descriptions of MIPS, LoongArch and benchmark platforms.
99 The configuration of the air quality numerical simulation system and simulation case
100 are also presented in Section 2. Section 3 describes porting and optimization of the
101 WRF-CAMx modelling system on MIPS and LoongArch CPU platforms. Section 4
102 analyzes the differences of model results between MIPS CPU platform and the
103 benchmark platform. Section 5 discusses MIPS and LoongArch CPUs performance in
104 scientific computing. The conclusions are presented in Section 6.

105

106 **2 Model and Porting Platform Description**

107 The air quality modeling system was constructed using the WRF v4.0 model
108 developed by National Center for Atmospheric Research (NCAR) (Skamarock et al.,
109 2019), and the CAMx v6.10 developed by Ramboll Environment (RAMBOLL
110 ENVIRON Inc., 2014), as shown in Figure 1. And the Loongson 3A4000 CPU platform
111 was chosen for the porting work in the study. This study introduced the porting of WRF-
112 CAMx modeling system to MIPS and LoongArch CPU platforms.



113

114 **Figure 1.** Framework of WRF-CAMx modeling system. The core modules have been
 115 ported to MIPS and LoongArch CPU platforms. The core modules are framed by red
 116 dashed line in the figure.

117 In Xi'an, China and Milan, Italy, the WRF-CAMx modelling system was applied ,
 118 enabling high-resolution hourly model output of pollutant concentration within specific
 119 local urban areas (Pepe et al., 2016; Yang et al., 2020). The modeling system is widely
 120 used to study the spatial-temporal variation of pollutant concentration and source
 121 apportionment, analyze the contribution of regional transport to pollution and
 122 investigate the impact of initial conditions and emissions on pollution simulation in key
 123 regions such as the North China Plain, Sichuan Basin, and Fenwei Plain (Bai et al.,
 124 2021; Zhen et al., 2023; Zhang et al., 2022; Xiao et al., 2021).

125

126 2.1 Description of WRF-CAMx modeling system

127 WRF and CAMx serve as the core components of the modeling system. WRF is a
 128 mesoscale numerical weather prediction system designed for atmospheric research and
 129 operational forecasting applications. Distinguished by its high temporal and spatial
 130 resolution, WRF is suitable for multi-scale simulations of short-term weather forecast,
 131 atmospheric process, and long-term climate, making it an essential tool in the
 132 meteorological and atmospheric research communities (Powers et al., 2017). In the
 133 modeling system, WRF provided gridded meteorological field data for air quality
 134 model CAMx. The relative humidity, a meteorological variable used in result validation
 135 is calculated using the wrf-python package (Official website: [https://wrf-](https://wrf-python.readthedocs.io)
 136 [python.readthedocs.io](https://wrf-python.readthedocs.io), last access: October 2023). CAMx is an atmospheric pollutant

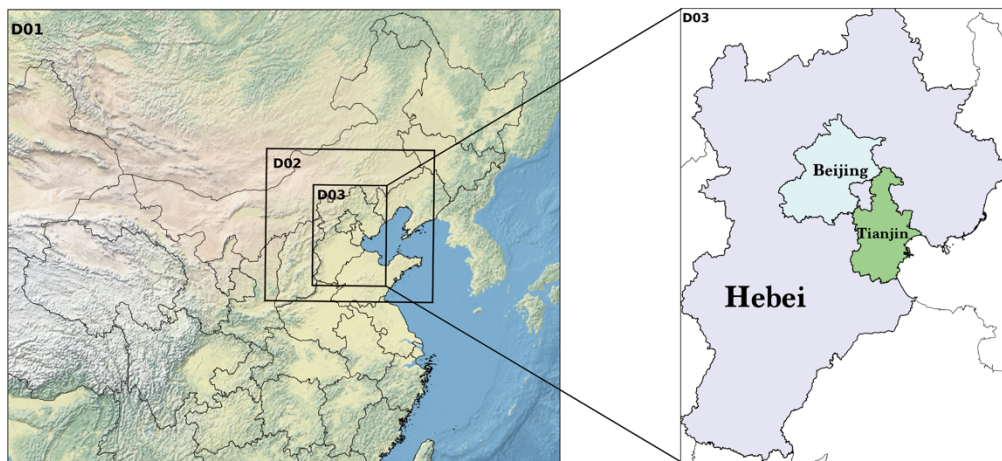
137 calculation model, which can be utilized for simulating and predicting the
138 concentrations of various air pollutants. The WRF and CAMx models are distinguished
139 by modularity and parallelism, using MPI in parallel computing, making them efficient
140 (Skamarock et al., 2019; RAMBOLL ENVIRON Inc., 2014).

141 In the modeling system, the SMOKE model and cmaq2camx program are used to
142 process emission data and provide model-ready gridded emission data for the CAMx
143 model. The wrfcamx program converts the WRF results into meteorological input files
144 which are compatible with CAMx. TUV is a radiation transfer model capable of
145 producing clean sky photolysis rate input files for the chemical mechanisms in CAMx,
146 and the o3map program prepares ozone column input files for TUV and CAMx. The
147 icbcprep program prepares initial and boundary condition files for CAMx with the
148 profile, and the effects of initial conditions have been studied by Xiao et al. (2021). The
149 camx2ioapi program converts the CAMx output files into netCDF format following the
150 Models-3/IO-API convention, and then uses NCL or other softwares to analyses the
151 model results.

152

153 **2.1.1 Model domain setup**

154 The model domain focusing on the Beijing-Tianjin-Hebei region has been set up
155 in this study. The WRF model has three nested domains with horizontal resolutions of
156 27km (D1), 9km (D2), and 3km (D3), as shown in Figure 2. The outer domain (D1)
157 covers most parts of China, and the inner domain (D3) covers Beijing, Tianjin, and
158 Hebei Province. The model domain is centered at (35°N, 110°E), with two true latitudes
159 located at 20°N and 50°N. The vertical resolution of WRF is 34 vertical layers. The
160 CAMx model has only one model domain, which is the innermost grid with a resolution
161 of 3km (D3), mainly covering the Beijing-Tianjin-Hebei region. The vertical resolution
162 of CAMx is 14 vertical layers, which is extracted from the WRF output files using the
163 wrfcamx module, and the lower seven layers of CAMx are same as those in the WRF
164 model.



165

166 **Figure 2.** The domains of three-level nested grids in the WRF-CAMx modelling system.

167 The respective horizontal resolutions are $27 \text{ km} \times 27 \text{ km}$ (D1), $9 \text{ km} \times 9 \text{ km}$ (D2), and

168 $3 \text{ km} \times 3 \text{ km}$ (D3).

169

170 **2.1.2 Model configuration**

171 Starting from 00:00 on November 3, 2020, until 24:00 on November 5, 2020, the

172 modelling system simulated the meteorological and air quality for a period of 72 hours,

173 represents a moderate-sized real scientific workload, which allows for testing in a short

174 time to validate the results and assess computational efficiency on the MIPS and

175 LoongArch platforms. For the meteorological model, the global meteorological initial

176 and boundary fields for the WRF model are derived from the NCEP Global Final

177 Reanalysis Data (FNL), with a spatial resolution of $0.5^\circ \times 0.5^\circ$ and a temporal resolution

178 of 6 hours. And the parameterization schemes of the WRF model used in the simulation

179 case are shown in Table 1.

180 For the air quality model, the meteorological files are provided by the WRF model

181 are used for the chemical transport module in CAMx. The emission inventory used in

182 the simulation case was obtained from Sun et al. (2022a). It contains basic emissions

183 from Sun et al. (2022b) and fugitive dust emission from bare ground surfaces. The

184 SMOKE model (v2.4) is used to process the emission inventory and provide gridded

185 emissions for CAMx. The parameterization schemes of the CAMx model used in the

186 simulation case are shown in Table 2.

187

188 **Table 1.** Parameterization schemes of WRF in research case.

Parameterization process	Scheme
Microphysics	WSM3
Longwave radiation	RRTM
Shortwave radiation	Dudhia
Land surface	Noah
Planetary boundary layer	YSU
Cumulus parameterization	Kain-Fritsch(new Eta)

189

190 **Table 2.** Parameterization schemes of CAMx in research case.

Parameterization process	Scheme
Horizontal Diffusion	PPM
Vertical Diffusion	K-theory
Dry Deposition	Zhang03
Gas-phase chemical mechanism	CB05
Aqueous aerosol chemistry	RADM-AQ
Inorganic gas-aerosol partitioning	ISORROPIA

191

192 **2.1.3 Statistical indicators for model results**

193 To quantify the differences in the model results between the MIPS and benchmark
194 platform, three statistical indicators are used to analyze the differences of concentration
195 time series: Mean Absolute Error (MAE), Root Mean Square Error (RMSE), and Mean
196 Absolute Percentage Error (MAPE). The MAPE quantifies the deviation between
197 computational differences and simulated values. The smaller these indicators, the better
198 accuracy and stability of scientific computing of the modeling system on the MIPS
199 platform. The calculation formulas for these statistical indicators are provided in
200 equations (1) to (3).

$$201 \quad MAE = \frac{1}{n} \sum_{i=1}^n |MIPS(i) - Base(i)| \quad (1)$$

$$202 \quad RMSE = \left[\frac{1}{n} \sum_{i=1}^n (MIPS(i) - Base(i))^2 \right]^{\frac{1}{2}} \quad (2)$$

$$203 \quad MAPE = \frac{1}{n} \sum_{i=1}^n \left| \frac{MIPS(i) - Base(i)}{MIPS(i)} \right| \times 100\% \quad (3)$$

204 In the equations, n represents the number of grids in the domain. $MIPS(i)$ represents the
205 simulated value of a certain grid on the MIPS platform, and $Base(i)$ represents the

206 baseline value of a certain grid on the benchmark platform.

207

208 **2.2 MIPS and LoongArch CPU platforms description**

209 Loongson CPU platform was chosen for the porting work in the study. Currently,
210 the Loongson processor family has three generations of CPU products, evolving from
211 single-core to multi-cores architectures and from experimental prototypes to mass-
212 produced industrial products (Hu et al., 2011). The Loongson-2 processor is a 64-bit
213 general-purpose RISC processor series which is compatible with MIPS instruction set.
214 It can be used in personal computers, mobile terminals, and various embedded
215 applications, running many operating systems such as Linux and Android smoothly
216 (Zhi et al., 2012). Wu et al. (2019) reports the application of the mesoscale model on
217 Loongson 2F CPU platform. The Loongson-3 processor features a scalable multi-core
218 architecture, targeting high-throughput data centers, high-performance scientific
219 computing, and other applications, with the significant advantage of achieving a high
220 peak performance-to-power ratio and striking a well-balanced trade-off between
221 performance and power consumption (Hu et al., 2009).

222 The Loongson 3A series are multi-core processors designed for high-performance
223 computers, featuring with high bandwidth, and low power consumption. The efficient
224 design solution and the advantage of high energy efficiency ratio make servers based
225 on Loongson CPUs highly competitive in performance, power consumption, and cost-
226 effectiveness (Li et al., 2014; Wang et al., 2014). In this study, the Loongson platform
227 uses the Debian Linux operating system, commercially known as Tongxin UOS
228 (<https://www.uniontech.com>, last access: January, 2024), and the Loongson 3A4000
229 processor, which is the first quad-core processor based on GS464v 64-bit
230 microarchitecture in Loongson 3 Processor Family. The main technical parameters of
231 Loongson 3A4000 CPU are shown in Table 3. Compared to previously released CPUs,
232 the processor improves frequency and performance by optimizing on-chip interconnect
233 and memory access path, integrating 64-bit DDR4 memory controller and on-chip
234 security mechanism. The Loongson 3A6000 CPU platform uses Loongnix, the open-
235 source community edition operating system released by Loongson

236 (<https://www.loongson.cn/system/loongnix>, last access: January, 2024), and the latest
 237 released Loongson 3A46000 processor, which is a quad-core processor based on LA664
 238 microarchitecture. The main technical parameters of Loongson 3A6000 CPU are shown
 239 in Table 3. The processor supports the LoongArch™ instruction set and hyper-threading,
 240 and the performance has significantly improved compared to the previously released
 241 processors (Hu et al., 2022).

242

243 **Table 3.** Main Parameters of Loongson 3A4000 CPU and Loongson 3A6000 CPU*

Main Parameters	Loongson 3A4000 CPU	Loongson 3A6000 CPU
Main Frequency	1.8GHz–2.0GHz	2.0GHz–2.5GHz
Peak Computing Speed	128Gflops@2.0GHz	240Gflops
Transistor Technology	28nm	12nm
Number of Cores	4	4(Physical) 8(Logical)
Processor Cores	MIPS64 compatible Support 128/256-bit vector instructions	support LoongArch™ Support 128/256-bit vector instructions
High-speed I/O	2 x 16-bit HyperTransport 3.0 control	1 x HyperTransport 3.0 control
Typical Power Consumption	<30W@1.5GHz <40W@1.8GHz <50W@2.0GHz	38W@2.5GHz

244 *source: <https://www.loongson.cn>, last access: January, 2024.

245

246 **2.3 Benchmark platform description**

247 This study uses an X86 CPU platform as benchmark platform compared to the
 248 MIPS and LoongArch CPU platforms. The benchmark platform is powered by Intel
 249 Xeon E5-2697 v4 CPU, with strong floating-point performance and many technical
 250 features such as Intel Turbo Boost Technology (Intel Inc., 2023). The Intel Xeon E5-
 251 2697 v4 CPU has 18 cores, with 2.3GHz base frequency and 3.6GHz maximum Turbo
 252 Boost frequency, 45 MB Intel Smart Cache and 145W design power consumption. The
 253 operating system is CentOS Linux 7.4.1708. The main information for all platforms is
 254 shown in Table 4.

255

256 **Table 4.** The comparison of main configuration between MIPS, LoongArch and X86
 257 platforms.

	MIPS Platform	LoongArch Paltform	X86 platform
CPU	Loongson 3A4000	Loongson 3A6000	Intel Xeon E5-2697 v4
Number of CPUs	1	1	1
Number of CPU cores	4	8	18
CPU Frequency	1.8GHz	2.0Ghz	2.3GHz
CPU instruction set	MIPS64	LoongArch™	X86_64
Operating system	Tongxin UOS	Loongnix	CentOS Linux 7.4.1708
Operating system kernel (Linux version)	4.19.0-loongson-3- desktop	4.19.0-19- loongson-3	3.10.0- 957.1.3.el7.x86_64

258

259

260 **2.4 The difference between MIPS, LoongArch and X86 platforms**

261 In this study, the numerical model's source code is written in Fortran, and
 262 commonly used compilers for X86 architecture include Intel Compiler, PGI and GNU
 263 Compiler. The compiler for MIPS platform is built using GCC 8.3 MIPS GNU/Linux
 264 cross-toolchain based on the open-source GNU Project, called MIPS GNU, and the
 265 latest version is 8.3. And the compiler for LoongArch platform is built using GCC 8.3
 266 LoongArch GNU/Linux cross-toolchain based on the open-source GNU Project, called
 267 LoongArch GNU, and the latest version is 8.3. The compiler for the benchmark
 268 platform is set to X86 GNU, and the version is also 8.3. Table 5 shows the differences
 269 between all platforms' GNU compilers in terms of applicable platforms. Compared to
 270 X86 GNU, the default compilation options of MIPS GNU compiler not only specify
 271 the platform architecture but also include additional instruction sets, such as atomic
 272 operation instruction set LLSC, shared library instruction set PLT, etc., which can
 273 optimize target programs compiled by GNU for MIPS architecture and improve

274 computational efficiency. And the default compilation options of LoongArch GNU
 275 compiler not only specify the platform architecture but also include target
 276 microarchitecture tuning option, which can also optimize target programs compiled by
 277 GNU for LoongArch architecture.

278 **Table 5.** Comparison of GNU compiler between MIPS, LoongArch and X86 CPU
 279 platforms.

Artitecture	MIPS64	LoongArch	x86_64
Compiler	MIPS GNU Fortran	LoongArch GNU Fortran	X86 GNU Fortran
Version	8.3	8.3	8.3
Target	mips64el-linux-gnuabi64	loongarch64-linux-gnu	x86_64-redhat-linux
Options (Architecture)	-march=mips64r2 -mabi=64	-march=loongarch64 -mabi=lp64d	-march=x86-64 -mtune=generic
Options (Instruction set)	-mllsc -mplt - mmadd4	-mtune=loongarch64	/
FLAGS(WRF)	-fconvert=big-endian -frecord-marker=4 -ffree-line-length-none -O2 -ftree-vectorize -funroll-loops		
FLAGS(CAMx)	-fconvert=big-endian -frecord-marker=4 -ffixed-line-length-none -fno-align-commons -O2		

280 The WRF-CAMx modeling system depends on several scientific computing
 281 libraries. Firstly, the general data format libraries netCDF and HDF5 are required to
 282 store the large-scale gridded data for the modeling system. NetCDF is a self-describing
 283 data format developed by NCAR/Unidata, primarily used for storing multidimensional
 284 array data in fields like meteorology and earth sciences (UCAR/Unidata, 2021). HDF5
 285 is a data format developed by HDF GROUP that supports complex data structures with
 286 multiple data types and multi-dimensional datasets (The HDF Group, 2019). In this
 287 study, netCDF-C (v4.8.1), netCDF-Fortran (v4.5.3), HDF5 (v1.12.1) and IOAPI (v3.1)
 288 were successfully installed on MIPS and LoongArch platforms by building from their
 289 sources, which are obtained from the official website.

290 The MPICH library is required to support parallel computing in the modeling
 291 system. In order to fully utilize computing resources, the method of MPI message
 292 communication is used in WRF and CAMx model (Wu et al., 2012). MPICH is an
 293 open-source, portable parallel computing library for implementing the MPI standard

294 (Amer et al., 2021). It supports inter-process communication and data exchange in the
295 parallel computing environment. Similarly, this study successfully installed MPICH
296 (v3.4) on MIPS and LoongArch platforms by building from its source. During the
297 compilation and installation of the mentioned libraries above, the configure tool was
298 used to check the basic information of the platform's CPU and compiler, and prepare
299 for compatibility with platform before compilation, the GNU compiler is used to
300 compile the source code of libraries, and the cmake tool is used to install the libraries.
301 Additionally, the same runtime environment as MIPS platform was also built on the
302 benchmark platform.

303

304 **3 Porting the WRF-CAMx modelling system on MIPS and LoongArch** 305 **CPU platforms**

306 The simulation result is influenced by several factors including processor
307 architecture, operating system, compiler, parallel environment, and scientific
308 computing libraries. In order to ensure stability and accuracy of numerical simulation,
309 the models should be adapted to the new runtime environment when porting across
310 platforms. Additionally, various operating systems have different tools, software and
311 libraries, which may impact the results of numerical simulations.

312 In this study, the runtime environment for WRF-CAMx modeling system was built
313 on MIPS and LoongArch platforms. The configuration files for making the models were
314 modified to fit the compilers of the Linux system on MIPS and LoongArch platforms.
315 In order to verify the stability of scientific computing on MIPS and LoongArch
316 platforms, a control experiment was set up on the benchmark platform, minimizing the
317 impact of other factors on simulation results of both platforms.

318 The WRF v4.0 and CAMx v6.10 were successfully deployed on MIPS and
319 LoongArch platforms through source code compilation and installation. In the WRF
320 model, the default options for GNU compiler which are suitable for MIPS and
321 LoongArch architecture CPUs are not provided in the configure file of the source code
322 package, and it is necessary to manually add information about the CPU architecture,

323 GNU compiler, and compilation flags on MIPS and LoongArch platforms. Table 5
324 provides the detailed information added in the configure file, mainly about MIPS and
325 LoongArch GNU Fortran. When compiling Fortran programs on MIPS and LoongArch
326 platforms, the MIPS and LoongArch GNU Fortran and necessary compilation flags
327 must be specified. These flags include common Fortran file format flags such as -
328 fconvert=big-endian and -frecord-marker=4, as well as optimization flags such as -O2
329 -ftree-vectorize -funroll-loops. By specifying the appropriate compiler and flags for
330 MIPS an LoongArch architectures, the configure tool will provide necessary settings to
331 compile WRF. Correspondingly, when compiling WRF on the benchmark platform, the
332 compilation flags are strictly consistent with those of MIPS and LoongArch CPU
333 platforms, which ensures that differences in simulation results of two platforms are
334 primarily attributed to the underlying hardware architecture rather than changes in
335 compilation settings.

336 In the CAMx model, the makefile provides information about parallelism and
337 compilers. Similarly, information about the CPU architecture, GNU compiler, and
338 compilation flags on MIPS and LoongArch platforms also needs to be added in the
339 makefile. For the detailed information added in the makefile, please refer to Table 5. So
340 far, the WRF-CAMx model has been successfully compiled and installed on the MIPS
341 and LoongArch platforms after modifications of the configuration files mentioned
342 above.

343

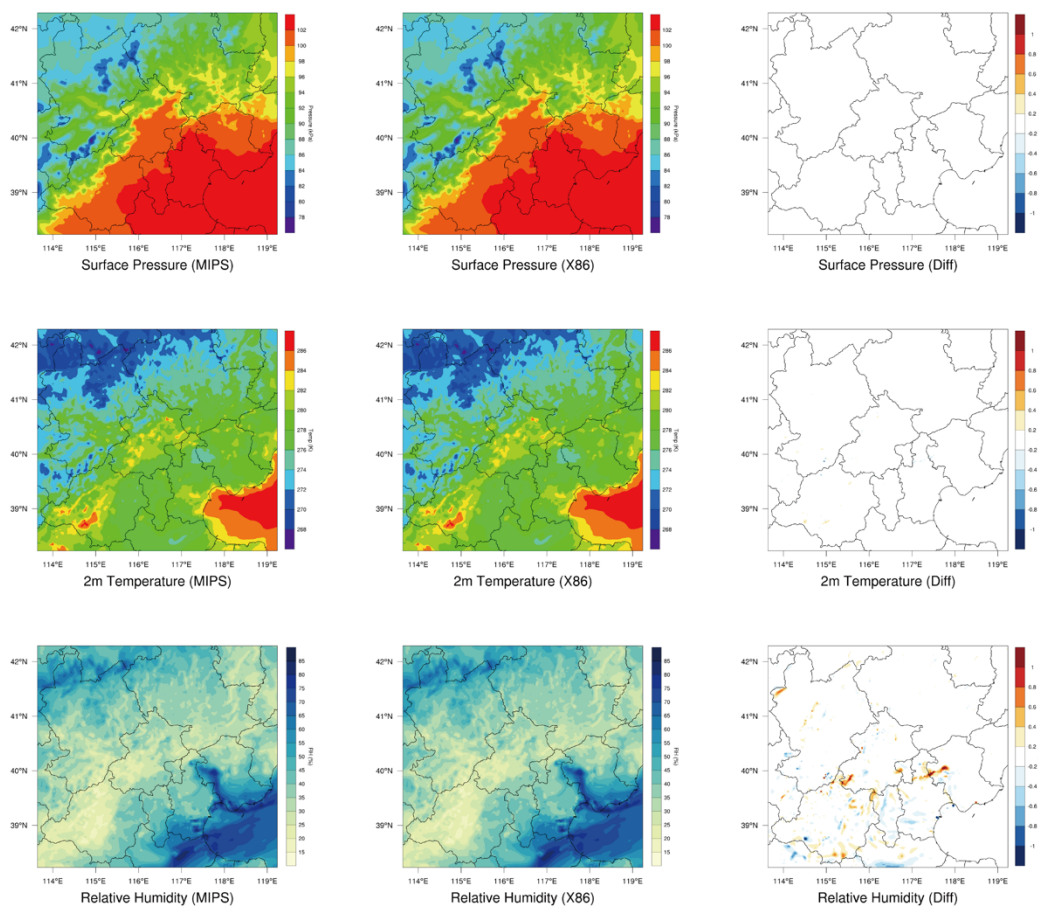
344 **4 The differences of model results on the two platforms**

345 **4.1 Validation of the spatial distribution**

346 A 72h simulation case has been designed to test the stability and availability of the
347 WRF-CAMx modeling system on the MIPS CPU platform in Beijing. By analyzing the
348 differences in simulation results and computing time, the accuracy and performance of
349 the modeling system on MIPS platform were evaluated, which further verifies the
350 feasibility and stability of the modeling system after porting to the MIPS platform.

351 Common meteorological variables, including 2-meter temperature, land surface

352 pressure, and relative humidity were selected to verify the WRF model results. Figure
 353 3 shows the spatial distribution of the four meteorological variables after 72 hours
 354 simulation on different platforms, as well as the absolute errors (AEs). The
 355 meteorological variables from the modeling system on the different platforms exhibit a
 356 generally consistent spatial distribution in the Beijing-Tianjin-Hebei regions shown in
 357 Figure 3.

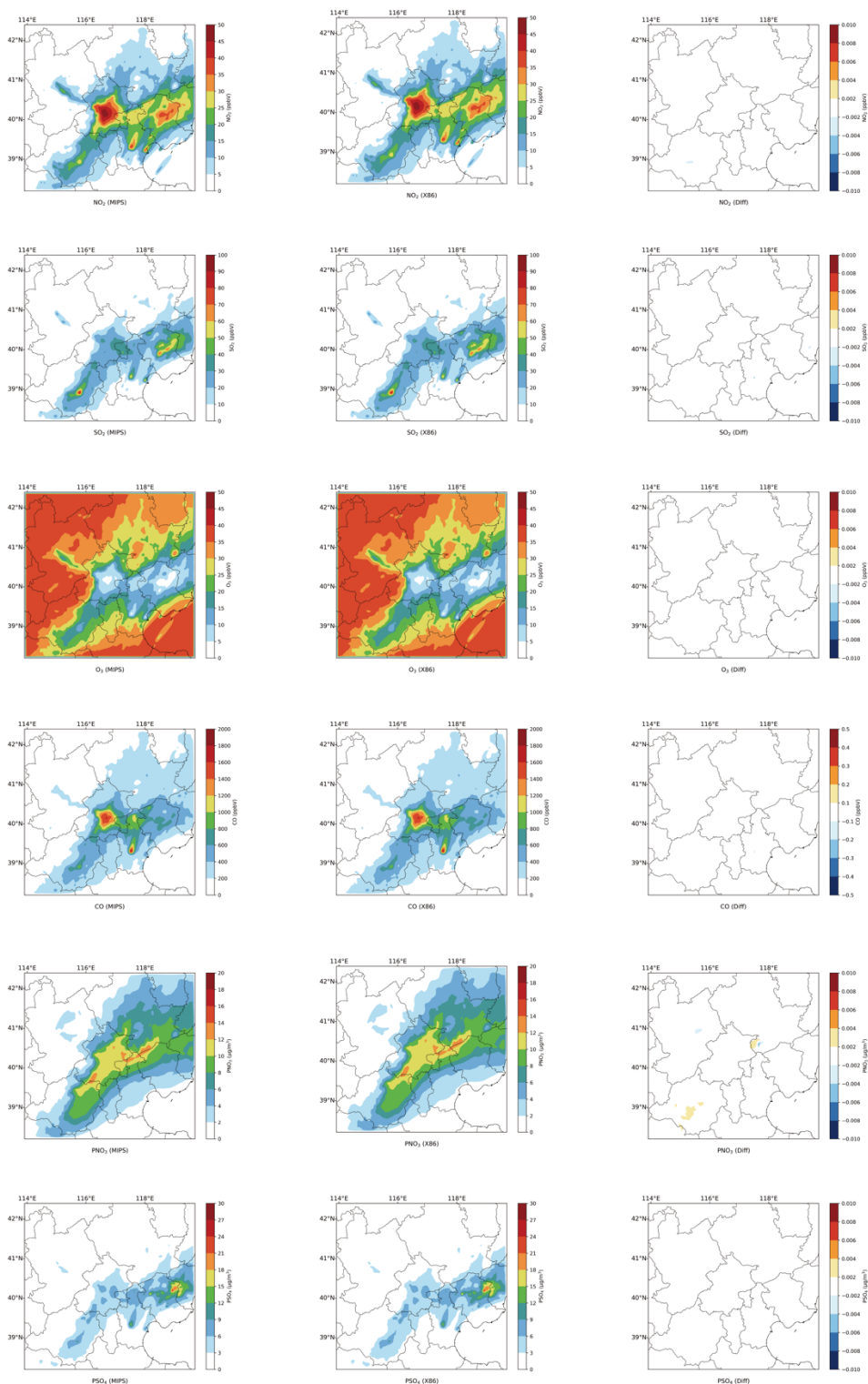


358
 359 **Figure 3.** Spatial distribution of 2m temperature, surface pressure, relative humidity
 360 from WRF. Left column, MIPS platform. Middle, the X86 platform. Right, the
 361 differences between the MIPS and benchmark(X86) platform.

362

363 Similarly, the NO₂, SO₂, O₃, CO, PNO₃ and PSO₄ were selected to verify the
 364 CAMx model results on the MIPS platform. Figure 4 shows the spatial distribution of
 365 the six species, as well as the absolute errors (AEs) between the two platforms after 72
 366 hours simulation. Simulating the 72h-case with four parallel processes using MPICH,

367 CAMx takes about 9h on Loongson 3A4000 CPU and 2.6h on Intel Xeon E5-2697 v4
 368 CPU. As shown in Figure 4, the spatial distribution of air pollution concentrations from
 369 the different platforms is essentially consistent, appearing very similar visually.

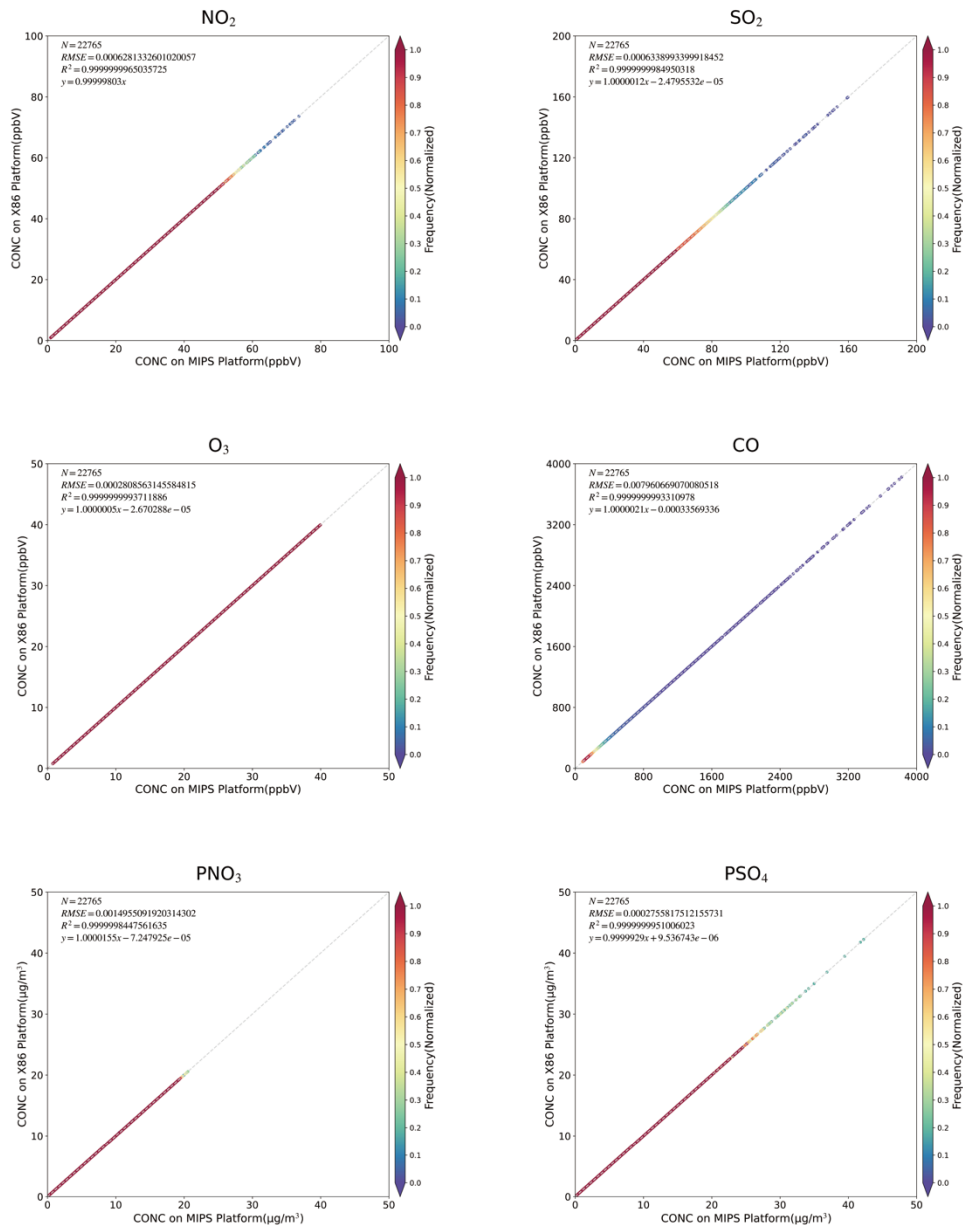


370

371 **Figure 4.** Spatial distribution of NO₂, SO₂, O₃, CO, PNO₃ and PSO₄ from CAMx on

372 MIPS and benchmark platform. Left column, MIPS platform. Middle, the X86 platform.
373 Right, the differences between the MIPS and benchmark(X86) platform.

374 As shown in Figure 5, the scatter plots between the two platform, it can be seen
375 that for the total of 22,765 grids within the 145x157 simulation domain, the root mean
376 square errors (RMSEs) of the six species between the MIPS platform and benchmark
377 platform are close to 0.001, which is essentially 0. The linear regression model was
378 used to fit the scatters, and the regression slopes for each species are nearly 1, with
379 intercepts close to 0, and the R2 values used for the goodness of fit are nearly 1. The
380 fitted lines closely coincide with the “ $y=x$ ” line, indicating that the differences between
381 the MIPS and X86 platform for each species are minimal to negligible.

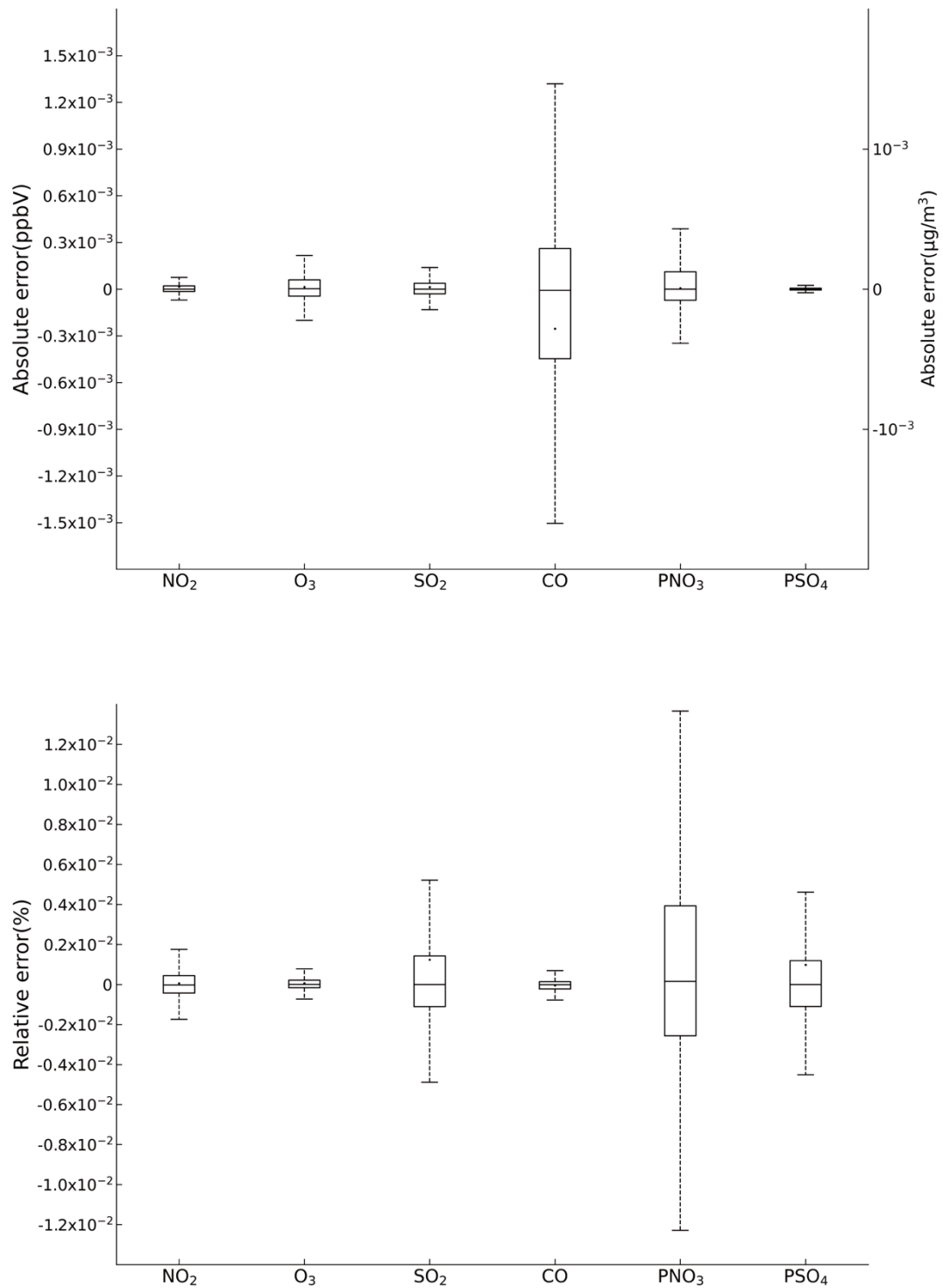


382

383 **Figure 5.** Scatter of grid concentrations for NO₂, SO₂, O₃, CO, PNO₃ and PSO₄ from
 384 CAMx on the MIPS and benchmark platform. The density of scatters is represented by
 385 the colors.

386 Figure 6 is the boxplots which show the absolute errors (AE) and relative errors
 387 (RE) of the six species between MIPS and benchmark platform. According to Figure 6,
 388 the absolute errors of the six species are generally in the range of $\pm 10^{-3}$ ppbv (parts per
 389 billion by volume; the unit of NO₂, SO₂, O₃ and CO concentration) or $\mu\text{g m}^{-3}$ (the unit
 390 of particle composition PNO₃ and PSO₄), and the relative errors are generally in the
 391 range of $\pm 0.01\%$. Specially for CO, it exhibits more pronounced AEs compared to other

392 species. In some grid boxes, the AEs between MIPS and benchmark platform exceed
393 the range of $\pm 10^{-3}$ ppbv, but they remain in the range of $\pm 10^{-2}$ ppbv. In summary, there
394 are some errors between the results of the modeling system on the MIPS and benchmark
395 platform during the porting process. However, these errors are relatively minor
396 compared to the numerical values. The reasons are attributed to the differences in the
397 CPU architecture and compiler characteristics between the two platforms, such as data
398 operations and precision running on different CPUs, which are primarily responsible
399 for the observed errors.



400

401 **Figure 6.** The absolute errors and relative errors for NO₂, SO₂, O₃, CO, PNO₃ and PSO₄
 402 concentration in all grids between the MIPS and benchmark platform.

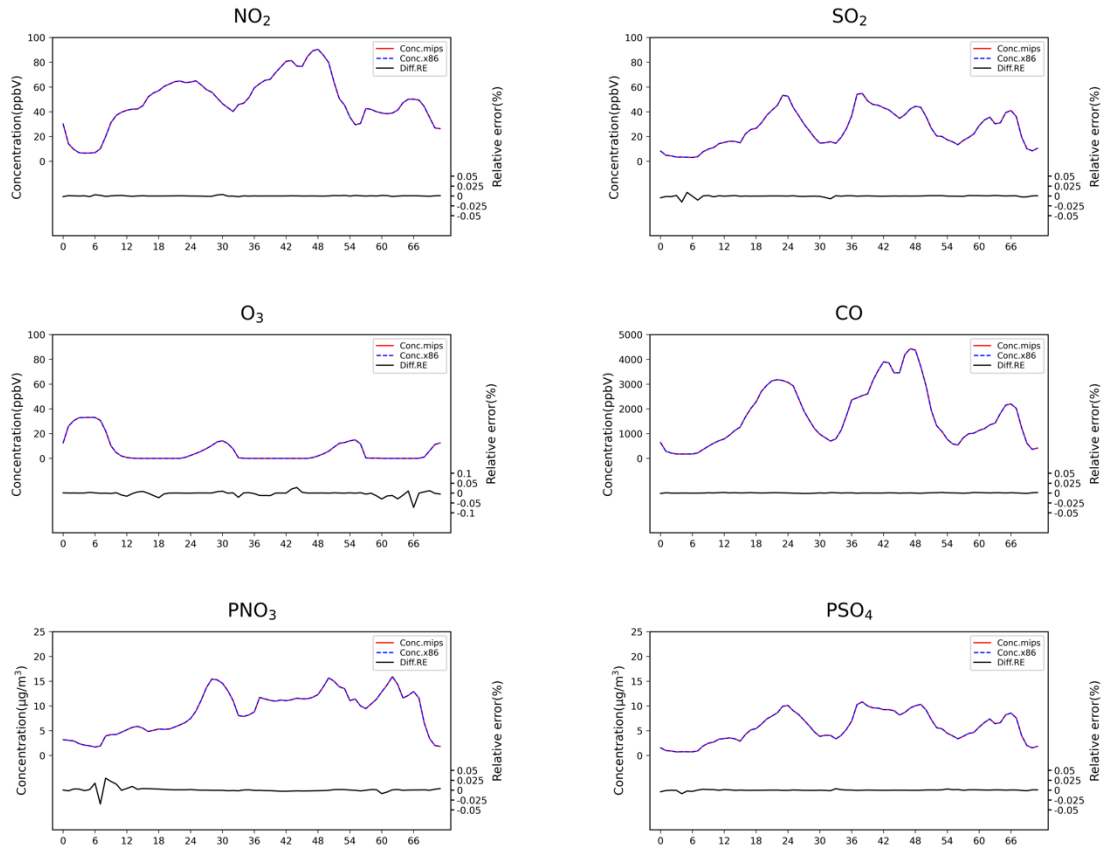
403 Additionally, random grids in the domain were selected to assess the precision of
 404 simulation results in localized regions. The positions of these grids were determined

405 based on 32 observation stations in Beijing, and the nearest grid was determined using
406 the Euclidean Shortest Distance in the domain. The station map is presented in Figure
407 S1 in the Supplement. The Taylor diagram is used to assess the precision of
408 concentrations for six species near the observation stations, and the scatters
409 representing the six species at 32 stations are highly overlapping. Statistical parameters
410 used in the Taylor diagram, such as the correlation coefficient (R) approaching 1,
411 normalized standard deviation (NSD) and normalized root mean square error (NRMSE)
412 approaching 0, indicate high precision of the simulation results at specific stations on
413 the MIPS platform.

414

415 **4.2 Validation of the temporal distribution from the two platform**

416 The time series of computational differences also be evaluated in this study.
417 Random grid in the domain was selected to examine the hourly concentrations of the
418 six species. Taking the example of the Beijing Olympic Center station (116.40°E,
419 39.99°N) from the National Standard Air Quality (NSAQ) stations, the time series of
420 hourly concentrations in the grid of the Beijing Olympic Center station and relative
421 errors between the MIPS and benchmark platform over the 72-hour period were shown
422 in Figure 7. As shown in Figure 7, it can be seen that the time series of the air pollutant
423 concentrations were highly consistent between the two platforms. In the 72-hour period,
424 the relative errors for NO₂, SO₂, CO and PSO₄ remain in ±0.025%. For PNO₃, the
425 relative errors remain in ±0.05%, and for O₃, they remain in ±0.1%. This indicates that
426 the errors caused by different architectures are within a reasonable range.

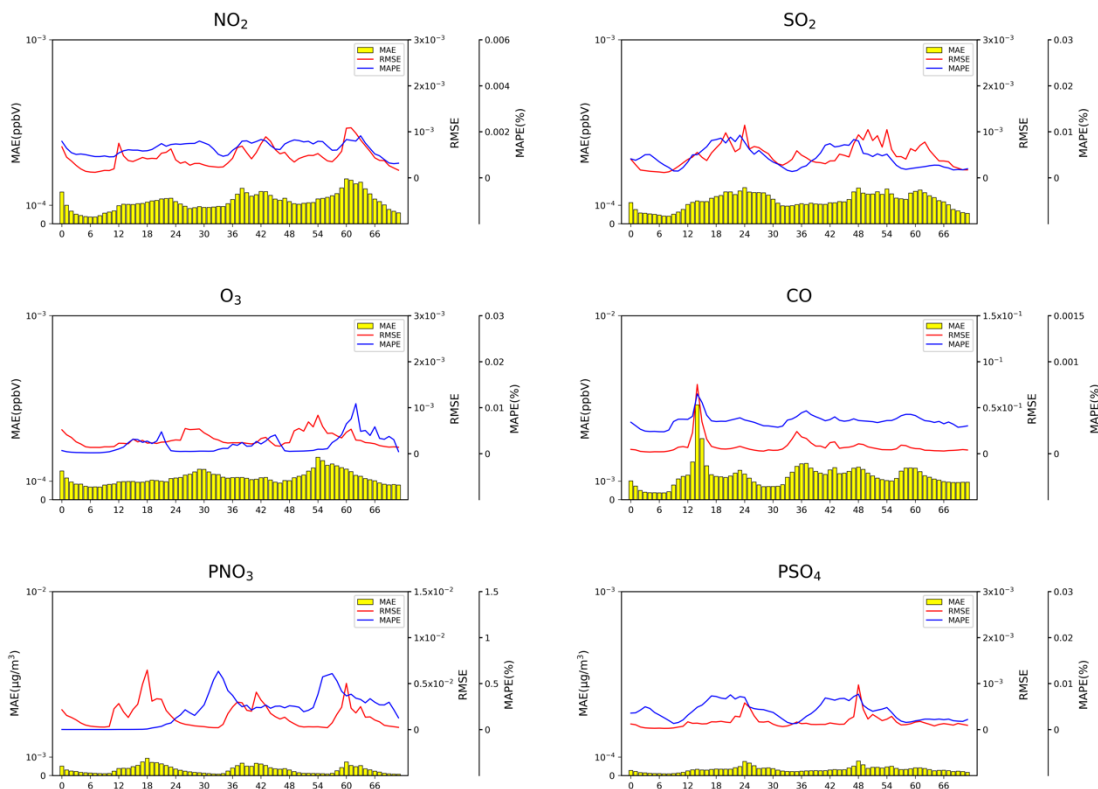


427

428 **Figure 7.** Time-series of NO₂, SO₂, O₃, CO, PNO₃ and PSO₄ concentrations and its
 429 relative errors (RE) at the Beijing Olympic Sports Center site between the MIPS and
 430 X86 platform. The red solid line and the blue dashed line, the CAMx model results on
 431 MIPS platform and X86 platform. The black solid line shows the relative errors (RE)
 432 between the MIPS and X86 platform.

433

434 Figure 8 shows the time series of the concentration and their statistical indicators,
 435 MAE, RMSE, and MAPE during the 72-hour simulation. As show in the figure, for
 436 NO₂, SO₂, O₃, and PSO₄, the MAEs are all below 10⁻³ ppbv (µg m⁻³), and the RMSEs
 437 are all below 10⁻³. The MAEs for CO and PNO₃ are below 10⁻² ppbv (µg m⁻³), and the
 438 RMSEs for PNO₃ are below 10⁻², while the RMSEs for CO are below 10⁻¹. This is
 439 because that PNO₃ and CO have relatively higher background concentrations compared
 440 to the other species. The MAPE of PNO₃ concentration mainly ranging in 0-0.5%, while
 441 the MAPE of CO concentration has the lowest values below 0.001%, and the other
 442 species are in the range of 0-0.01%. Overall, the above time-series analysis verifies the
 443 accuracy and stability of the modeling system on the MIPS platform.



444

445 **Figure 8.** Time series of MAEs, RMSEs and MAPEs for NO₂, SO₂, O₃, CO, PNO₃ and
 446 PSO₄ concentration in the 72h simulation. The yellow bar, the MAE. The red lines,
 447 RMSE, the blue lines, MAPE.

448

449 In this study, the evaluation method proposed by Wang et al. (2021) was also used
 450 to assess the scientific applicability of the model results on the MIPS platform. The
 451 Root Mean Square Errors (RMSEs) for NO₂, SO₂, O₃, CO, PNO₃ and PSO₄
 452 concentration between the MIPS and benchmark platform were computed, along with
 453 the standard deviations (stds) used to describe the spatial variation of species, and the
 454 ratio of RMSE to std, as shown in Table 6. The differences of the four species between
 455 the two platforms are negligible compared to their own spatial variations. Therefore,
 456 the results on the MIPS platform meet the accuracy requirements for research purpose.

457

458 **Table 6.** RMSE, std, RMSE/std for NO₂, SO₂, O₃, CO, PNO₃ and PSO₄.

	Differences in results	Spatial variation	RMSE/std
	RMSE	std	
NO ₂	6.3×10^{-7}	0.01	5.9×10^{-5}

O₃	2.8×10^{-7}	0.01	2.5×10^{-5}
SO₂	6.3×10^{-7}	0.02	3.9×10^{-5}
CO	7.9×10^{-6}	0.30	2.6×10^{-5}
PNO₃	1.5×10^{-3}	3.8	3.9×10^{-4}
PSO₄	2.7×10^{-4}	3.9	6.9×10^{-5}

459

460 In fact, the differences in model results cannot be completely eliminated, primarily
461 due to the varying CPU architectures and compilers. In the practical applications,
462 compared with the errors arising from the inherent uncertainties of the modeling system
463 and the input data, the differences of model results between different platforms can even
464 be considered negligible. The comprehensive analysis demonstrates that the results of
465 the WRF-CAMx modeling system on the MIPS CPU platform are reasonable.

466

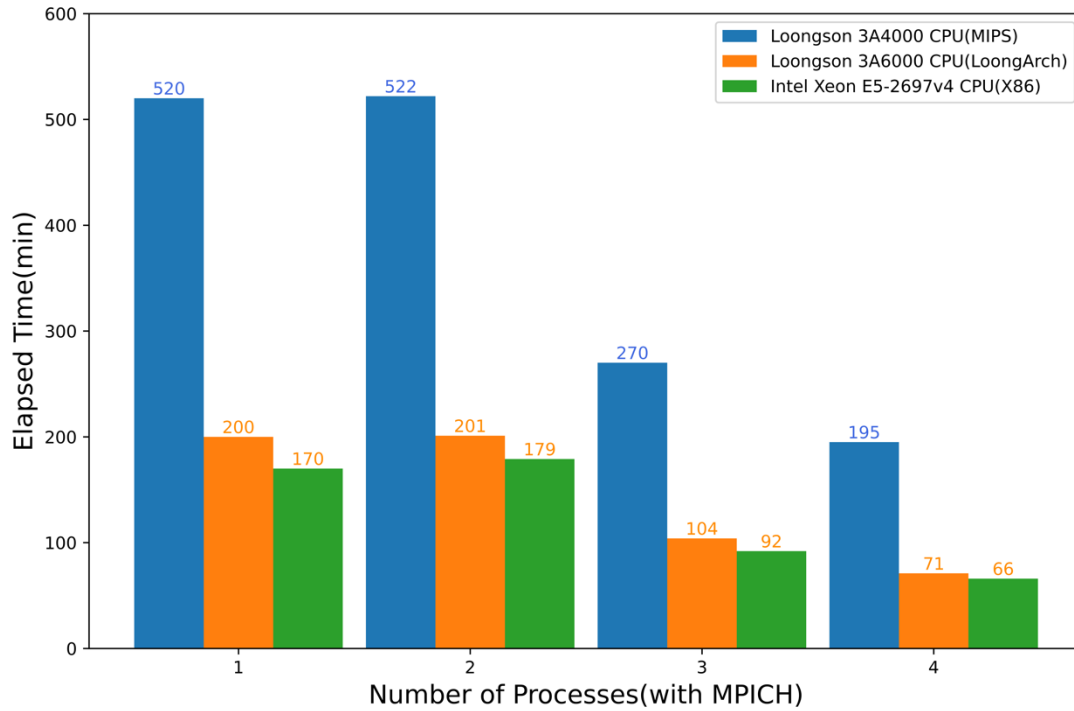
467 **5 The evaluation about computational performance**

468 Scientific computing involves a significant amount of floating-point operations,
469 and the floating-point computational capability is a crucial indicator for CPU
470 performance. In this study, the simulation case was configured to conduct parallel
471 computing tests on the MIPS, LoongArch and benchmark platform. These tests
472 included assessing the CPU's single-core performance with the non-parallel model and
473 the platform's parallel performance with the parallel model using multiple processes.
474 The time of CAMx model running simulation case for 24 hours in the modeling system
475 are shown in Figure 9. From the figure, it can be observed that under single-core
476 conditions, the computing capability of the MIPS platform for CAMx is approximately
477 one-third of the X86 benchmark platform, and the LoongArch platform is slightly lower
478 than the X86 benchmark platform.

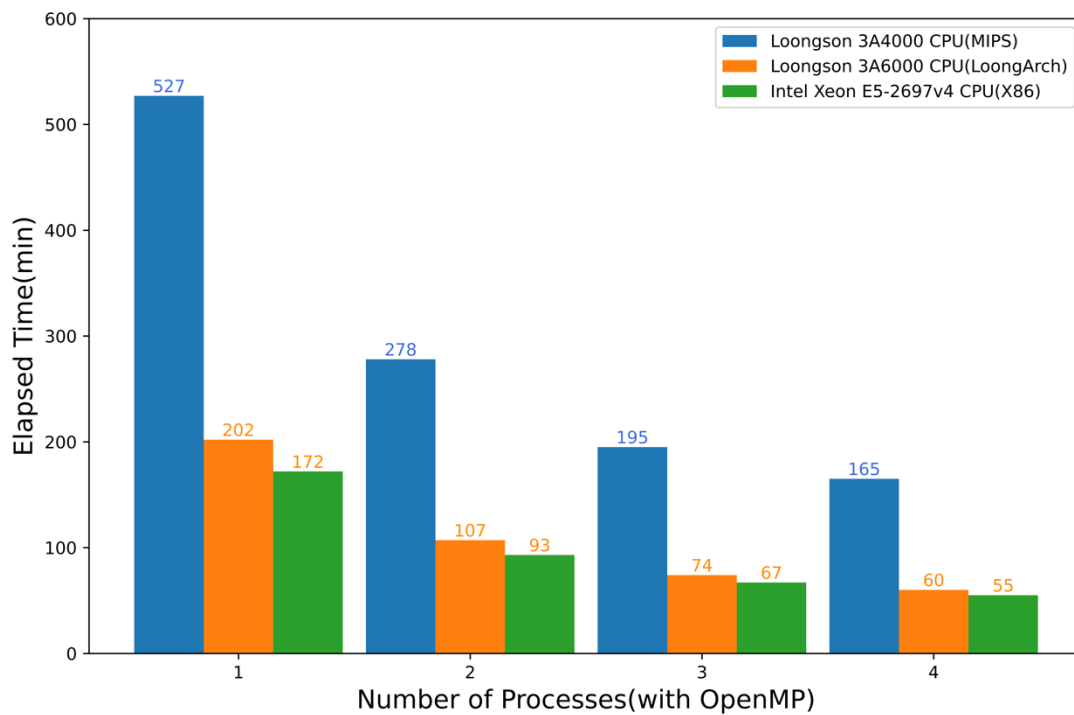
479 It's worth noting that the simulation time of the CAMx model for running with two
480 processes in parallel and running in non-parallel remains approximately consistent.
481 This is because the MPI used in CAMx is designed using a "master/slave" parallel
482 processing approach, and a process is allocated for input/output and message
483 communication during the runtime (Cao K et al., 2023). This process doesn't perform
484 any simulation in the model. Therefore, the time required for parallelism of two

485 processes is comparable to the non-parallelism, and in some cases, it might even be
486 slightly longer due to the overhead of MPI communication. Compared to non-parallel,
487 the speedup of the MIPS platform with four-process parallelism using MPICH3 is
488 approximately 2.8, while using OpenMP is about 2.9, and the speedup of the
489 LoongArch platform with four-process parallelism using MPICH3 is approximately 2.8,
490 while using OpenMP is about 2.9. For the X86 benchmark platform, running with four
491 processes in parallel using MPICH3 has a speedup of approximately 2.7.

492 Additionally, the performance of the MIPS platform significantly decreases when
493 the number of parallel processes exceeds 4. This is because the modeling system
494 involves compute-intensive tasks. The Loongson 3A4000 CPU has four cores, and
495 when the number of processes called by MPI matches the number of CPU cores, the
496 CPU utilization can approach 100%. Further increasing the number of processes, the
497 cores will compete for CPU resources, resulting in additional overhead and reduced
498 computational efficiency. As for LoongArch platform, the performance slightly
499 decreases when the number of parallel processes exceeds 4. The Loongson 3A6000
500 CPU has four physical cores and eight logical cores, and when the number of processes
501 called by MPI matches the number of physical cores, the computational load is evenly
502 distributed across each core. Although the Loongson 3A6000 supports hyper-threading,
503 further increasing the number of processes, CPU starts to schedule logical cores to
504 allocate computational load. Thread scheduling will result in additional overhead and
505 reduced computational efficiency. This explains why the elapsed time is slightly higher
506 when CAMx running with 5 parallel processes compared to 4 parallel processes as
507 shown in the Supplementary Material.



508



509

510 **Figure 9.** Elapsed time of CAMx model running simulation case with MPICH and
 511 OpenMP for 24 hours on the MIPS, LoongArch and benchmark platforms.

512

513 In the recent years, the Longsoon CPUs have been continuously upgraded.
 514 Compared to the previous generations of products, the performance of Loongson CPUs
 515 has shown significant improvement. Wu et al. (2019) simulated a nested domain

516 covering Beijing for 48 hours using the MM5 model on the Longsoon 3A quad-core
517 CPU platform. The results showed that the computational capacity of the Longsoon 3A
518 platform for the MM5 model is approximately equivalent to around 1/12 of the Intel
519 Core 2 Q8400 quad-core CPU, which was released in the same year. In the study of
520 Luo et al. (2011), a comparison between Loongson 3A and Intel i5 was made by running
521 NPB benchmark on each platform. The results shows that the performance of the 3A is
522 nearly one-tenth of that of the i5. The rapid development of Loongson CPUs has
523 provided a strong hardware foundation for the application of numerical simulation and
524 scientific computing on MIPS and LoongArch architecture CPU platforms. The
525 adaptation and optimization of the models based on RISC CPUs will also be an
526 important research direction in the future.

527

528 **6 Conclusion**

529 This study describes the application of the WRF-CAMx model on the MIPS CPU
530 platform. The platform used in this study is Loongson 3A4000 quad-core CPU with the
531 main frequency of 1.8-2.0GHz, which can offer a peak operational speed of 128GFlops.
532 It is equipped with the MIPS GNU compiler. The benchmark platform used the Intel
533 Xeon E5-2697 v4 CPU along with the same version of X86 GNU compiler. Based on
534 the characteristics of CPU architecture and compiler, this study has successfully
535 completed the construction of runtime environment for the WRF-CAMx modeling
536 system. The application of an air quality modelling system based on WRF-CAMx was
537 successfully tested using a 72-hour simulation case in the Beijing-Tianjin-Hebei region.

538 The results showed that the spatial distribution of the meteorological variables and
539 air pollutant species was nearly identical, with relative errors in the range of $\pm 0.1\%$.
540 Statistically, the maximum MAEs of major species ranged from 10^{-3} to 10^{-2} ppbv ($\mu\text{g m}^{-3}$),
541 the maximum RMSEs ranged from 10^{-2} to 10^{-1} ppbv ($\mu\text{g m}^{-3}$), and the MAPEs
542 remained within 0.5%, that the differences caused by the architectures and compilers
543 were within a reasonable range. Simulating a 2h-case with four parallel processes using
544 MPICH, CAMx takes about 15.2min on Loongson 3A4000 CPU and 4.8 min on Intel

545 Xeon E5-2697 v4 CPU. In terms of single-core CPU performance, the single-core
546 computing capability of Loongson 3A4000 CPU for the WRF-CAMx modeling system
547 is about one-third of Intel Xeon E5-2697 v4 CPU.

548 Currently, Loongson Technology has focused on the LoongArch architecture and
549 it has been used in the latest product. It is foreseeable that the LoongArch architecture
550 will lead to more significant performance improvements. In the future, as the numerical
551 models become more complex and computational scales become larger, more models
552 will be tested on high-performance computing platforms equipped with the LoongArch
553 architecture CPUs.

554

555 **Code and data availability.** The source codes of CAMx version 6.10 are available at
556 <https://camx-wp.azurewebsites.net/download/source> (ENVIRON, 2023). The datasets
557 related to this paper and the binary executable files of CAMx for MIPS and LoongArch
558 CPUs are available online via ZENODO (<https://doi.org/10.5281/zenodo.10722127>).

559

560 **Supplement.** The supplement related to this article is available on-line.

561

562 **Author contributions.** ZB and QW conducted the simulation and prepared the materials.
563 QW planned and organized the project. ZB and QW completed the porting and
564 application of the model for MIPS and LoongArch CPUs. YS collected and prepared
565 the emission data for the simulation. ZB, QW, KC, and HC participated in the
566 discussion.

567

568 **Acknowledgements.** The National Key R&D Program of China (2020YFA0607804)
569 and the Beijing Advanced Innovation Program for Land Surface funded this work. The
570 research is supported by the High Performance Scientific Computing Center (HSCC)
571 of Beijing Normal University.

572

573 **Competing interests.** The contact author has declared that none of the authors has any
574 competing interests.

576 **References**

- 577 Amer, A., Balaji, P., Bland, W., Gropp, W., Guo, Y., Latham, R., Lu, H., Oden, L., Pena, A. J.,
 578 Raffanetti, K., Seo, S., Si, M., Thakur, R., Zhang, J., and Zhao, X.: MPICH User's Guide
 579 Version 3.4, available at: <https://www.mpich.org/static/downloads/3.4/mpich-3.4-userguide.pdf>,
 580 2021.
- 581 Appel, K. W., Napelenok, S. L., Foley, K. M., Pye, H. O. T., Hogrefe, C., Luecken, D. J., Bash, J.
 582 O., Roselle, S. J., Pleim, J. E., Foroutan, H., Hutzell, W. T., Pouliot, G. A., Sarwar, G., Fahey, K.
 583 M., Gantt, B., Gilliam, R. C., Heath, N. K., Kang, D., Mathur, R., and Schwede, D. B.: Description
 584 and evaluation of the Community Multiscale Air Quality (CMAQ) modeling system version 5.1,
 585 Geoscientific Model Development, 10, 1703–1732, <https://doi.org/10.5194/gmd-10-1703-2017>,
 586 2017.
- 587 Appel, K. W., Bash, J. O., Fahey, K. M., Foley, K. M., Gilliam, R. C., Hogrefe, C., Hutzell, W. T.,
 588 Kang, D., Mathur, R., Murphy, B. N., Napelenok, S. L., Nolte, C. G., Pleim, J. E., Pouliot, G. A.,
 589 Pye, H. O. T., Ran, L., Roselle, S. J., Sarwar, G., Schwede, D. B., Sidi, F. I., Spero, T. L., and
 590 Wong, D. C.: The Community Multiscale Air Quality (CMAQ) model versions 5.3 and 5.3.1:
 591 system updates and evaluation, Geoscientific Model Development, 14, 2867–2897,
 592 <https://doi.org/10.5194/gmd-14-2867-2021>, 2021.
- 593 Bai, X., Tian, H., Liu, X., Wu, B., Liu, S., Hao, Y., Luo, L., Liu, W., Zhao, S., Lin, S., Hao, J., Guo,
 594 Z., and Lv, Y.: Spatial-temporal variation characteristics of air pollution and apportionment of
 595 contributions by different sources in Shanxi province of China, Atmospheric Environment, 244,
 596 117926, <https://doi.org/10.1016/j.atmosenv.2020.117926>, 2021.
- 597 Cao, K., Wu, Q., Wang, L., Wang, N., Cheng, H., Tang, X., Li, D., and Wang, L.: GPU-HADVPPM
 598 V1.0: a high-efficiency parallel GPU design of the piecewise parabolic method (PPM) for
 599 horizontal advection in an air quality model (CAMx V6.10), Geosci. Model Dev., 16, 4367–4383,
 600 <https://doi.org/10.5194/gmd-16-4367-2023>, 2023.
- 601 Chen, H. S., Wang, Z. F., Li, J., Tang, X., Ge, B. Z., Wu, X. L., Wild, O., and Carmichael, G. R.:
 602 GNAQPMS-Hg v1.0, a global nested atmospheric mercury transport model: model description,
 603 evaluation and application to trans-boundary transport of Chinese anthropogenic emissions,
 604 Geoscientific Model Development, 8, 2857–2876, <https://doi.org/10.5194/gmd-8-2857-2015>,
 605 2015.
- 606 George, A. D.: An overview of RISC vs. CISC, in: [1990] Proceedings. The Twenty-Second
 607 Southeastern Symposium on System Theory, The Twenty-Second Southeastern Symposium on
 608 System Theory, Cookeville, TN, USA, 436–438, <https://doi.org/10.1109/SSST.1990.138185>,
 609 1990.
- 610 Hennessy, J., Jouppi, N., Przybylski, S., Rowen, C., Gross, T., Baskett, F., and Gill, J.: MIPS: A
 611 microprocessor architecture, SIGMICRO Newsl., 13, 17–22,
 612 <https://doi.org/10.1145/1014194.800930>, 1982.
- 613 Hu, W., Wang, J., Gao, X., Chen, Y., Liu, Q., and Li, G.: Godson-3: A Scalable Multicore RISC
 614 Processor with x86 Emulation, IEEE Micro, 29, 17–29, <https://doi.org/10.1109/MM.2009.30>,
 615 2009.
- 616 Hu, W., Zhang, Y., and Fu, J.: An introduction to CPU and DSP design in China, Sci. China Inf. Sci.,
 617 59, 1–8, <https://doi.org/10.1007/s11432-015-5431-6>, 2016.

618 Hu, W., Gao, X., and Zhang, G.: Building the software ecosystem for the Loongson instruction set
619 architecture, *Information and Communications Technology and Policy*, 43–48, 2022 (in Chinese).

620 Hu, W.-W., Gao, Y.-P., Chen, T.-S., and Xiao, J.-H.: The Godson Processors: Its Research,
621 Development, and Contributions, *J. Comput. Sci. Technol.*, 26, 363–372,
622 <https://doi.org/10.1007/s11390-011-1139-2>, 2011.

623 Intel Inc.: Intel® 64 and IA-32 Architectures Software Developer’s Manual, Volume 1: Ba
624 sic Architecture, available at: [https://www.intel.com/content/www/us/en/developer/articles/te
625 chnical/intel-sdm.html](https://www.intel.com/content/www/us/en/developer/articles/technical/intel-sdm.html), 2023.

626 Li, L., Chen, Z., and Wang, S.: Power Consumption and Analysis of Server Based on Loongson
627 CPU No. 3, *Information Technology & Standardization*, 46–50, 2014 (in Chinese).

628 Liu, Y., Ye, K., and Xu, C.-Z.: Performance Evaluation of Various RISC Processor Systems: A Case
629 Study on ARM, MIPS and RISC-V, in: *Cloud Computing – CLOUD 2021*, Cham, 61–74,
630 https://doi.org/10.1007/978-3-030-96326-2_5, 2022.

631 Luo, Q., Kong, C., Cai, Y., and Liu, G.: Performance Evaluation of OpenMP Constructs and Kernel
632 Benchmarks on a Loongson-3A Quad-Core SMP System, in: *2011 12th International Conference
633 on Parallel and Distributed Computing, Applications and Technologies, 2011 12th International
634 Conference on Parallel and Distributed Computing, Applications and Technologies*, 191–196,
635 <https://doi.org/10.1109/PDCAT.2011.66>, 2011.

636 Mallach, E. G.: RISC: Evaluation and Selection, *Journal of Information Systems Management*, 8,
637 8–16, <https://doi.org/10.1080/07399019108964978>, 1991.

638 Michalakes, J., Chen, S., Dudhia, J., Hart, L., Klemp, J., Middlecoff, J., and Skamarock, W.:
639 Development of a next-generation regional weather research and forecast model, in:
640 *Developments in Teracomputing, WORLD SCIENTIFIC*, 269–276,
641 https://doi.org/10.1142/9789812799685_0024, 2001.

642 MIPS Technology Inc.: MIPS Architecture For Programmers Volume I-A, available at:
643 <https://www.mips.com/products/architectures/mips64>, 2014.

644 Pepe, N., Pirovano, G., Lonati, G., Balzarini, A., Toppetti, A., Riva, G. M., and Bedogni, M.:
645 Development and application of a high resolution hybrid modelling system for the evaluation of
646 urban air quality, *Atmospheric Environment*, 141, 297–311,
647 <https://doi.org/10.1016/j.atmosenv.2016.06.071>, 2016.

648 Powers, J. G., Klemp, J. B., Skamarock, W. C., Davis, C. A., Dudhia, J., Gill, D. O., Coen, J. L.,
649 Gochis, D. J., Ahmadov, R., Peckham, S. E., Grell, G. A., Michalakes, J., Trahan, S., Benjamin,
650 S. G., Alexander, C. R., Dimego, G. J., Wang, W., Schwartz, C. S., Romine, G. S., Liu, Z., Snyder,
651 C., Chen, F., Barlage, M. J., Yu, W., and Duda, M. G.: The Weather Research and Forecasting
652 Model: Overview, System Efforts, and Future Directions, *Bulletin of the American
653 Meteorological Society*, 98, 1717–1737, <https://doi.org/10.1175/BAMS-D-15-00308.1>, 2017.

654 RAMBOLL ENVIRON Inc.: CAMx User’s Guide Version 6.1, available at: [https://camx-
655 wp.azurewebsites.net/Files/CAMxUsersGuide_v6.10.pdf](https://camx-wp.azurewebsites.net/Files/CAMxUsersGuide_v6.10.pdf), 2014.

656 Shi, Z.: Technology comparison and research of RISC and CISC, *China Science and Technology
657 Information*, 131–132, 2008 (in Chinese).

658 Skamarock, C., Klemp, B., Dudhia, J., Gill, O., Liu, Z., Berner, J., Wang, W., Powers, G., Duda, G.,
659 Barker, D., and Huang, X.: A Description of the Advanced Research WRF Model Version 4,
660 <https://doi.org/10.5065/1dfh-6p97>, 2019.

661 Sun Y.: Research on the contribution of soil fugitive dust in Beijing based on satellite identification

662 and numerical simulation technology, Master, Beijing Normal University, <https://etdlib.bnu.edu.cn>,
663 2022a.

664 Sun, Y., Wu, Q., Wang, L., Zhang, B., Yan, P., Wang, L., Cheng, H., Lv, M., Wang, N., and Ma, S.:
665 Weather Reduced the Annual Heavy Pollution Days after 2016 in Beijing, *Sola*, 18, 135–139,
666 <https://doi.org/10.2151/sola.2022-022>, 2022b.

667 The HDF Group: HDF5 User’s Guide Version 1.1, available at:
668 <https://portal.hdfgroup.org/display/HDF5/HDF5+User+Guides>, 2019.

669 UCAR/Unidata: NetCDF User’s Guide Version 1.1, available at: <https://docs.unidata.ucar.edu/nug> ,
670 2021.

671 Wang, K., Gao, C., Wu, K., Liu, K., Wang, H., Dan, M., Ji, X., and Tong, Q.: ISAT v2.0: an
672 integrated tool for nested-domain configurations and model-ready emission inventories for WRF-
673 AQM, *Geoscientific Model Development*, 16, 1961–1973, [https://doi.org/10.5194/gmd-16-1961-](https://doi.org/10.5194/gmd-16-1961-2023)
674 [2023](https://doi.org/10.5194/gmd-16-1961-2023), 2023.

675 Wang, P., Jiang, J., Lin, P., Ding, M., Wei, J., Zhang, F., Zhao, L., Li, Y., Yu, Z., Zheng, W., Yu, Y.,
676 Chi, X., and Liu, H.: The GPU version of LASG/IAP Climate System Ocean Model version 3
677 (LICOM3) under the heterogeneous-compute interface for portability (HIP) framework and its
678 large-scale application, *Geosci. Model Dev.*, 14, 2781–2799, [https://doi.org/10.5194/gmd-14-](https://doi.org/10.5194/gmd-14-2781-2021)
679 [2781-2021](https://doi.org/10.5194/gmd-14-2781-2021), 2021.

680 Wang, S., Li, L., and Chen, Z.: The Test and Analysis on Memory Access Performance Based on
681 Loongson CPU, *Information Technology & Standardization*, 32–36, 2014 (in Chinese).

682 Wang, Z., Xie, F., Wang, X., An, J., and Zhu, J.: Development and Application of Nested Air Quality
683 Prediction Modeling System, *Chinese Journal of Atmospheric Sciences*, 778–790,
684 <http://dx.doi.org/10.3878/j.issn.1006-9895.2006.05.07>, 2006.

685 Wu, Q. and Cheng, H.: Transplantation and application of mesoscale mode on Loongson CPU
686 platform, *Journal of Beijing Normal University (Natural Science)*, 55, 11–18,
687 <https://doi.org/10.16360/j.cnki.jbnuns.2019.01.002>, 2019.

688 Wu, Q., Xu, W., Shi, A., Li, Y., Zhao, X., Wang, Z., Li, J., and Wang, L.: Air quality forecast of
689 PM10 in Beijing with Community Multi-scale Air Quality Modeling (CMAQ) system: emission
690 and improvement, *Geoscientific Model Development*, 7, 2243–2259,
691 <https://doi.org/10.5194/gmd-7-2243-2014>, 2014.

692 Wu, Y., Xu, G., Zhao, Y., and Tan, Y.: Parallel Processing on WRF Meteorological Data Using
693 MPICH, in: 2012 Sixth International Conference on Internet Computing for Science and
694 Engineering, 2012 Sixth International Conference on Internet Computing for Science and
695 Engineering, titleTranslation:, 262–265, <https://doi.org/10.1109/ICICSE.2012.12>, 2012.

696 Xiao, H., Wu, Q., Yang, X., Wang, L., and Cheng, H.: Numerical study of the effects of initial
697 conditions and emissions on PM2.5 concentration simulations with CAMx v6.1: a Xi’an case
698 study, *Geoscientific Model Development*, 14, 223–238, [https://doi.org/10.5194/gmd-14-223-](https://doi.org/10.5194/gmd-14-223-2021)
699 [2021](https://doi.org/10.5194/gmd-14-223-2021), 2021.

700 Yang, X., Xiao, H., Wu, Q., Wang, L., Guo, Q., Cheng, H., Wang, R., and Tang, Z.: Numerical study
701 of air pollution over a typical basin topography: Source appointment of fine particulate matter
702 during one severe haze in the megacity Xi’an, *Science of The Total Environment*, 708, 135213,
703 <https://doi.org/10.1016/j.scitotenv.2019.135213>, 2020.

704 Zhang, Y., Bocquet, M., Mallet, V., Seigneur, C., and Baklanov, A.: Real-time air quality forecasting,
705 part I: History, techniques, and current status, *Atmospheric Environment*, 60, 632–655,

706 <https://doi.org/10.1016/j.atmosenv.2012.06.031>, 2012.

707 Zhang, Z., Wang, X., Cheng, S., Guan, P., Zhang, H., Shan, C., and Fu, Y.: Investigation on the
708 difference of PM_{2.5} transport flux between the North China Plain and the Sichuan Basin,
709 Atmospheric Environment, 271, 118922, <https://doi.org/10.1016/j.atmosenv.2021.118922>, 2022.

710 Zhen, J., Guan, P., Yang, R., and Zhai, M.: Transport matrix of PM_{2.5} in Beijing-Tianjin-Hebei and
711 Yangtze River Delta regions: Assessing the contributions from emission reduction and
712 meteorological conditions, Atmospheric Environment, 304, 119775,
713 <https://doi.org/10.1016/j.atmosenv.2023.119775>, 2023.

714 Zhi, Y. and Xu, J.: Android transplantation and analysis based on Loongson, in: 2012 International
715 Conference on Information Management, Innovation Management and Industrial Engineering,
716 2012 International Conference on Information Management, Innovation Management and
717 Industrial Engineering, 59–61, <https://doi.org/10.1109/ICIM.2012.6339777>, 2012.